

Aggressive aerosol mitigation policies reduce chances of keeping global warming to below 2C.

R. Wood^{1*}, M. A. Vogt¹, and I. L. McCoy^{2,3,4}

¹Department of Atmospheric Sciences, University of Washington, Seattle, WA, USA

²Cooperative Institute for Research in Environmental Sciences, University of Colorado, Boulder, CO, USA

³National Oceanic and Atmospheric Administration, Chemical Sciences Laboratory, Boulder, CO, USA

⁴Cooperative Programs for the Advancement of Earth System Science, University Corporation for Atmospheric Research, Boulder, CO, USA

Key Points:

- Aerosol forcing changes are isolated from CMIP6 projected scenarios using an approximate partial radiative perturbation method.
- Aerosol-cloud interactions dominate future aerosol forcing changes from cleanup policies over the period 2020-2050.
- Likelihood of maintaining global warming to below 2C will be strongly reduced by implementing aggressive near-term aerosol cleanup policies.

*Department of Atmospheric Sciences, University of Washington, Seattle

Corresponding author: Robert Wood, robwood2@uw.edu

Abstract

Aerosol increases over the 20th century delayed the rate at which Earth warmed as a result of increases in greenhouse gases (GHGs). Aggressive aerosol mitigation policies arrested aerosol radiative forcing from ~ 1980 to ~ 2010 . Recent evidence supports decreases in forcing magnitude since then. Using the approximate partial radiative perturbation (APRP) method, future shortwave aerosol effective radiative forcing changes are isolated from other shortwave changes in an 18-member ensemble of ScenarioMIP projections from phase 6 of the Coupled Model Intercomparison Project (CMIP6). APRP-derived near-term (2020-2050) aerosol forcing trends are correlated with published model emulation values but are 30-50% weaker. Differences are likely explained by location shifts of aerosol-impacting emissions and their resultant influences on susceptible clouds. Despite weaker changes, implementation of aggressive aerosol cleanup policies will have a major impact on global warming rates over 2020-2050. APRP-derived aerosol radiative forcings are used together with a forcing and impulse response model to estimate global temperature trends. Strong mitigation of GHGs, as in SSP1-2.6, likely prevents warming exceeding 2C since preindustrial but the strong aerosol cleanup in this scenario increases the probability of exceeding 2C by 2050 from near zero without aerosol changes to 6% with cleanup. When the same aerosol forcing is applied to a more likely GHG forcing scenario (i.e., SSP2-4.5), aggressive aerosol cleanup more than doubles the probability of reaching 2C by 2050 from 30% to 80%. It is thus critical to quantify and simulate the impacts of changes in aerosol radiative forcing over the next few decades.

Plain Language Summary

Over the 20th century, fossil fuel burning led to increased concentrations of greenhouse gases (GHGs) and small particles known as aerosols. Aerosols scatter sunlight back to space and enhance cloud brightness and longevity, thus cooling Earth. The amount of warming since the pre-industrial depends upon both GHGs and aerosol. After ~ 1980 , air quality improvements led to a reduction in this cooling effect, unmasking some of the GHG potential to warm the planet. This has reinforced the importance of understanding the interplay between aerosols and GHGs in climate projections. To examine this sensitivity, we use a set of global climate model simulations forced by a variety of future GHG and aerosol concentration based on plausible socioeconomic pathways. Shifts in the location of regional aerosol emissions has an impact on the global climate, influencing the accuracy of our predictions for Earth's future warming as measured by the probability of increasing global temperatures by 2C by 2050 compared to pre-industrial. Under plausible GHG scenarios, aggressive aerosol cleanup policies can more than double the probability of crossing this threshold. This emphasizes the urgency of improving our simulations in order to accurately predict and quantify the impact of aerosols over the next few decades.

1 Introduction

The increase of atmospheric aerosol loading over the 20th century delayed the rate at which Earth's global mean temperature increased due to increases in well-mixed greenhouse gases (Meehl et al., 2004). Although the magnitude of present day aerosol forcing is uncertain (Bellouin et al., 2020), recent studies suggest aerosol loading globally reached a peak close to the turn of the 21st century (Quaas et al., 2022) due to air quality cleanup policies designed to mitigate the deleterious health impacts of particulate matter. Anthropogenic aerosol forcing associated with increased aerosol loading arises from aerosol-radiation interactions, i.e., changes in clear sky scattering and absorption, and from cloud-mediated effects known as aerosol-cloud interactions (Bellouin et al., 2020). Aerosol-cloud interactions comprise increases in cloud droplet concentration that increase the reflection of sunlight even without cloud macrophysical changes, a phenomenon known

66 as the Twomey effect. In addition, increases in droplet concentration can induce adjust-
67 ments in cloud condensate (liquid water) and potentially cloud cover (Seinfeld et al., 2016;
68 Bellouin et al., 2020). Marine low clouds downstream of major industrialized regions have
69 seen declines in cloud droplet concentration (D. T. McCoy et al., 2018) that indicate a
70 reduction in the Twomey effect, and the hemispheric contrast in cloud droplet concen-
71 tration between the polluted Northern and more pristine Southern Hemispheres has de-
72 creased significantly since 2000 (Cao et al., 2023). We are now in an era where the rate
73 of change of aerosol radiative forcing is positive, which *ceteris paribus* must increase the
74 rate of global warming (Dvorak et al., 2022). Thus, it is important that climate change
75 risk assessments include the impacts of changing atmospheric aerosol and precursor emis-
76 sions (Persad et al., 2022).

77 Even with overall emissions fixed, a shift in the emission *location* can change the
78 global aerosol radiative forcing (Persad & Caldeira, 2018), and changes in the efficacy
79 of a given radiative forcing (Hansen et al., 2005) can result in different global mean tem-
80 perature change per unit of radiative forcing. The Scenario Model Intercomparison Project
81 (ScenarioMIP, O'Neill et al., 2016) within Phase 6 of the Coupled Model Intercompar-
82 ison Project (CMIP6) provides a suite of plausible future emissions trajectories (shared
83 socioeconomic pathways) under different assumptions regarding social and economic devel-
84 opment, including climate mitigation efforts. There are very different motivations for
85 air quality cleanup vs climate mitigation efforts, and these are associated with vastly dif-
86 ferent short term (decadal) costs and benefits to individual nations. Thus, future aerosol
87 changes are not necessarily coupled to future well-mixed greenhouse gas (WGMHG) emis-
88 sions. The prior two decades are an example of this decoupling: air quality cleanup ef-
89 forts have proceeded rapidly but mitigation of WGMHG emissions has been extremely
90 limited. This situation may well continue through the next few decades, although this
91 is not at all certain since rapid industrialization of Africa and South America has the
92 potential to stall aerosol emission reductions globally (Feng et al., 2019).

93 There is a general consensus that the impacts of climate change are likely to be-
94 come increasingly dire if global warming is allowed to exceed 2C above the preindustrial
95 (Masson-Delmotte et al., 2021). In 2020, the global mean temperature of the Earth was
96 close to $\sim 1.2\text{C}$ above the preindustrial (Morice et al., 2021), and global mean warming
97 rates over the last few decades¹ have averaged about 0.2 K decade^{-1} . Thus, it is impor-
98 tant to quantify the potential impact of different aerosol cleanup policies on the global
99 rate of warming over the coming few decades. Here, we use an 18-member ensemble of
100 ScenarioMIP projections (O'Neill et al., 2016) from CMIP6 models (Eyring et al., 2016)
101 to explore how aerosol cleanup may influence the probability that global warming ex-
102 ceeds 2C by 2050. Section 2 describes the data and methods used. Section 2.2 describes
103 a novel approach that applies the approximate partial radiative perturbation (APRP)
104 method (Taylor et al., 2007) to the multimodel mean output data and partitions future
105 SW radiative changes into temperature-driven and aerosol-driven components, from which
106 we estimate future aerosol radiative forcing and compare it with the published estimates
107 for four shared socioeconomic pathways. Section 4 then uses the derived aerosol radia-
108 tive forcing estimates together with a forcing and response two-level energy balance model
109 (Geoffroy et al., 2013) to explore the impacts of different future aerosol pathways for aerosol
110 cleanup. Section 5 provides an assessment of the implications of the findings and the main
111 conclusions from the study.

¹ See NOAA National Centers for Environmental Information, Monthly Global Climate Re-
port for August 2023, published online September 2023, retrieved on September 27, 2023 from
<https://www.ncei.noaa.gov/access/monitoring/monthly-report/global/202308>.

2 Materials and Methods

2.1 CMIP6 ScenarioMIP Simulations

Climate model projections from four Tier-1 ScenarioMIP scenarios from CMIP6 are analyzed here. Each scenario has a distinct SSP and level of forcing following the Representative Concentration Pathways (RCPs) used for previous CMIPs (O'Neill et al., 2016; Riahi et al., 2017). The SSPs include differences in societal development related to concerns around climate change. Low numbered SSPs (e.g., SSP1: *Sustainability*, SSP2: *Middle of the Road*) have fewer challenges to climate mitigation while higher SSPs have more (e.g., SSP3: *Regional Rivalry*, SSP5: *Fossil-fueled Development*) (Riahi et al., 2017). Each of the SSPs also includes projections of future emissions of aerosol and precursor gases. These somewhat parallel the WMGHG changes in that SSPs with aggressive greenhouse gas mitigation tend to have aggressive aerosol reduction. As discussed in the introduction, it is far from clear that there will be such a tight coupling between aerosol and WMGHG mitigation in the coming decades. In this study, we will decouple future changes in aerosol from future changes in WMGHG to allow, for example, an aggressive aerosol cleanup strategy to be applied to less aggressive WMGHG mitigation scenarios (or vice versa).

SSP1-2.6 uses the RCP2.6 pathway, is the most weakly-forced scenario considered (experiencing less than 2C warming by 2100 in the multi-model mean), and undergoes aggressive aerosol cleanup. SSP2-4.5 undergoes intermediate radiative forcing, is an update to RCP4.5, and has a less rapid reduction in aerosol compared to other SSPs. SSP3-7.0 has a higher radiative forcing (an update to RCP7.0). In particular, it has large land use changes and maintains high emissions of short lived climate forcers (e.g., aerosols) until 2100. Finally, SSP5-8.5 is the most strongly-forced scenario considered, an update to RCP8.5.

Our analysis focuses on changes between the present day (2015-2025) and the future decades of the 21st century using composites from 18 CMIP6 models (more details in the supplementary material). All currently available models with outputs necessary for estimating aerosol contributions to the top of atmosphere (TOA) energy budget are included. We use aerosol optical depth at 550 nm wavelength (*AOD*) as the measure of aerosol loading as it is available for the most models. For reference, global changes in key quantities for the four scenarios by the end of the 21st century are listed in Table S2 of I. L. McCoy et al. (2022).

The trends in *AOD*, which are primarily driven by changes in anthropogenic aerosol emissions (Turnock et al., 2020), differ strongly across the four scenarios (Fig. 1a). The trends in the future *AOD* changes in different SSPs are largely independent of global warming trends (Fig 1b) because warming is *primarily* driven by changes in WMGHGs, with a weaker modulation by aerosol. Aerosol trend differences are most evident over the next few decades, so we focus primarily on the period 2020-2050, where aerosol cleanup is likely to have the largest impact on warming rates. SSP1-2.6 has the most aggressive reduction in *AOD*, with rapid cleanup occurring prior to 2050, while SSP2-4.5 has a weaker, but steadier decline in *AOD* that extends beyond 2050. SSP3-7.0 essentially has no aerosol mitigation and has close to zero *AOD* trend over the 21st century. SSP5-8.5 is very similar to SSP2-4.5 prior to 2050 before *AOD* reduction ceases until after 2070 (not shown). These changes are consistent with projected emissions of aerosol and precursor gases (most importantly SO_2 and VOCs) (Turnock et al., 2020). We can therefore identify three broad *aerosol cleanup pathways*: (a) deep and rapid cleanup (SSP1-2.6); (b) slow and steady cleanup (SSP2-4.5); (c) no cleanup (SSP3-7.0).

2.2 Approximate Partial Radiative Perturbation analysis

Partial radiative perturbation (PRP) analysis (e.g., Colman & McAvaney, 1997) is an offline method to compute feedbacks (e.g., water vapor, lapse rate, cloud, etc.) in

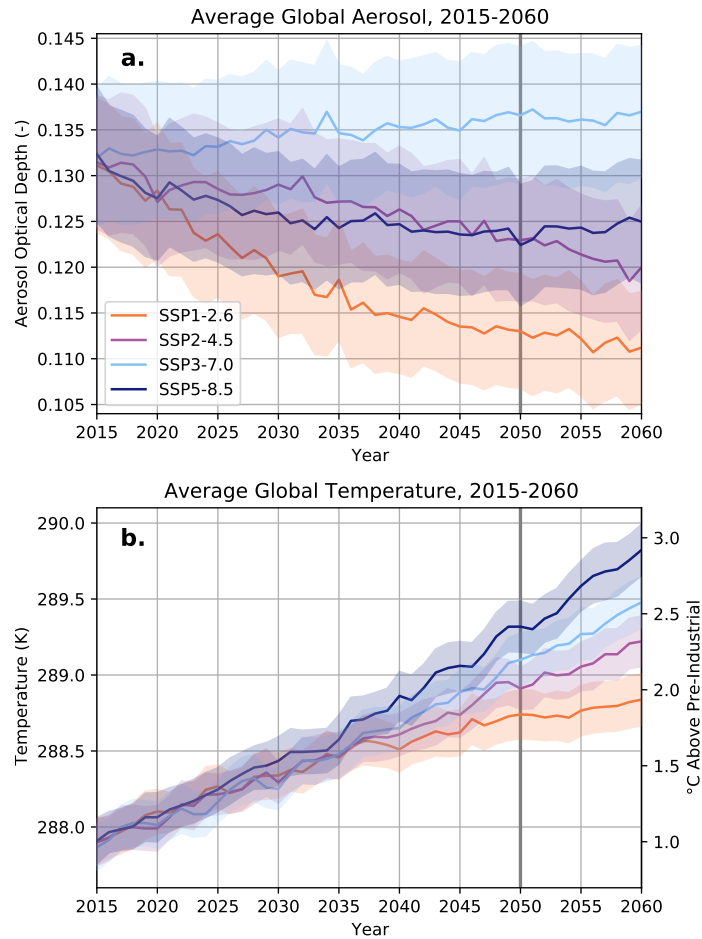


Figure 1. Ensemble annual and global mean (a) aerosol optical depth (*AOD*) and (b) surface air temperature from the CMIP6 models used in this study. For (b), the absolute temperature is indicated on the left axis and the temperature relative to the preindustrial baseline on the right axis.

162 response to some forcing from a climate model simulation by examining the TOA radiative changes when the "control" and "perturbed" model fields are interchanged. For PRP,
 163 radiative changes when the "control" and "perturbed" model fields are interchanged. For PRP,
 164 dedicated calls to the model's radiative transfer scheme must be made, and a large volume of model output data is required. A simpler method, that targets contributions to
 165 TOA shortwave perturbations, and can be applied to standard (typically monthly mean) model outputs, is known as the approximate PRP (APRP) method (Taylor et al., 2007).
 166 We use the APRP code provided by Mark Zelinka². The APRP method apportions changes in TOA SW radiation (ΔSW) to changes in cloudy sky SW (ΔC), non-cloudy sky SW
 167 (ΔN), and to changes in surface albedo (ΔS):
 168
 169
 170

$$\Delta SW = \Delta C + \Delta N + \Delta S \quad (1)$$

171 The APRP method further breaks the cloudy and non-cloudy sky components into
 172 respective changes due to scattering and absorption, and, for ΔC , changes in cloud amount.

² See <https://doi.org/10.5281/zenodo.5514142>

173
 174

Surface albedo influences on ΔSW are broken down into changes of surface albedo under cloudy sky and non-cloudy sky conditions separately:

$$\Delta C = \Delta C_{\text{scat}} + \Delta C_{\text{abs}} + \Delta C_{\text{amt}} \quad (2)$$

$$\Delta N = \Delta N_{\text{scat}} + \Delta N_{\text{abs}} \quad (3)$$

$$\Delta S = \Delta S_{\text{clld}} + \Delta S_{\text{clr}} \quad (4)$$

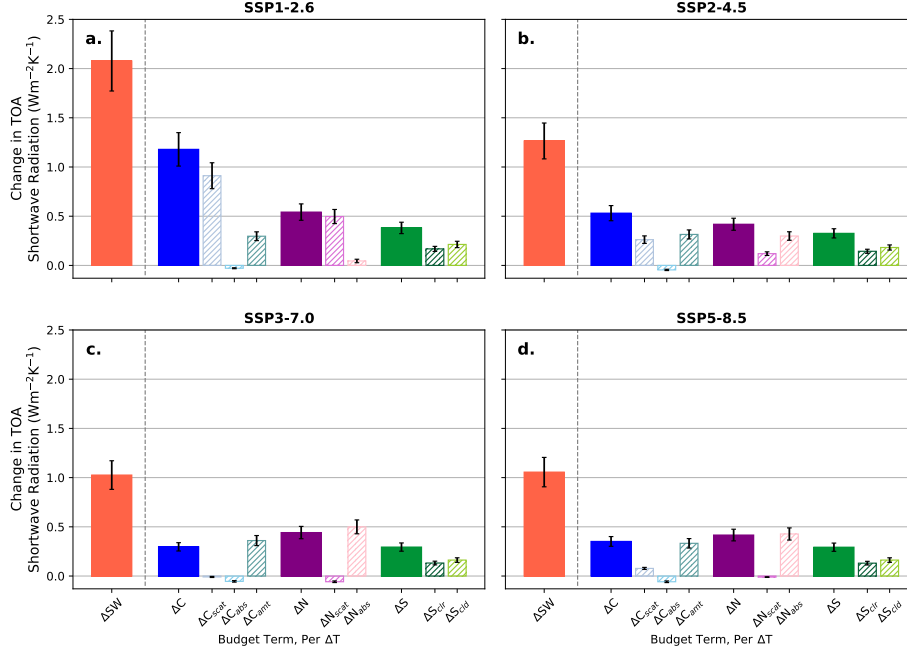


Figure 2. Apportionment of changes in TOA SW radiation (ΔSW , solid red bars) over the 21st century (2090–2100 minus 2015–2025) into changes in cloudy sky (ΔC , solid blue), clear sky (ΔN , solid purple), and changes in surface albedo (ΔS , solid green) deduced from the APRP analysis. Changes are all normalized by the global mean surface air temperature changes over the same period, ΔT . Hatched bars indicate further breakdown of these components (see Eqns. 2, 3, and 4). Bars represent multi-model means while error bars show 2 standard errors ($\sim 95\%$ confidence) based on the variability in the multi-model mean 10-year periods propagated through the change and normalization calculations.

 175
 176
 177
 178
 179
 180
 181
 182

Figure 2 shows these changes in TOA SW over the 21st century normalized by the global mean surface air temperature changes ΔT over the same period. Importantly, differences in $\Delta SW/\Delta T$ across the four SSPs (solid red bars) are driven primarily by changes in the cloudy sky (ΔC , solid blue bars), with a much smaller influence of variability in the non-cloudy sky and surface albedo. Given that surface air temperature changes over the 21st century vary considerably across the SSPs (Fig. 1b, Table S1), the relative invariance in $\Delta S/\Delta T$ across the SSPs (Fig. 2) indicates that surface albedo-driven TOA SW changes are largely a temperature-mediated feedback.

 183
 184
 185
 186

From 2020 to 2100, 99% of the variance in ΔSW across all four SSPs is explained by ΔT and ΔAOD as predictors in a multiple linear regression model (Fig. 3). Thus, most of the variance in ΔSW can be explained by a linear sum of a temperature mediated feedback and an aerosol-driven SW response. The predictor variables ΔT and ΔAOD

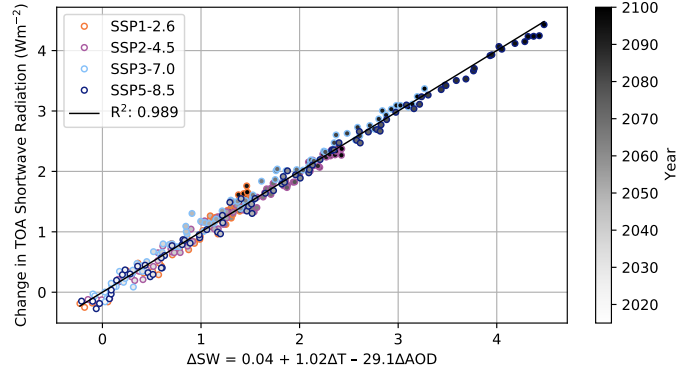


Figure 3. Annual mean TOA SW differences from those in 2015 (ΔSW) plotted as a function of annual mean ΔAOD and ΔT . A single regression line is fitted, explaining 99% of the variance using ΔT and ΔAOD as predictors.

187 are uncorrelated ($r^2=0.01$), so multicollinearity issues (e.g., Qu et al., 2015), where predictor
 188 variables are highly correlated, is not a concern here. To further explore the temper-
 189 ature and aerosol-driven SW changes, we also conduct linear regression analysis of
 190 the individual component SW changes (ΔC , ΔN , and ΔS) to isolate changes that dep-
 191 end upon ΔAOD from those due to temperature-mediated climate feedbacks (Fig. 4).
 192 Like that for the overall ΔSW , these individual component regressions (which include
 193 all four SSPs) also explain a very high fraction of the variance in the SW APRP com-
 194 ponents. Each of ΔC , ΔN , and ΔS is regressed against ΔT and ΔAOD . Normalizing
 195 by ΔT means that the temperature mediated sensitivities are, by construction, identi-
 196 cal across SSPs (Fig. 4) because we use all four SSP time series in each regression. Sep-
 197 arate regressions for each SSP produce very similar ΔT sensitivities (not shown). Aerosol-
 198 mediated changes differ widely across SSPs (Fig. 4). The T -mediated components of the
 199 SW component changes can be removed to isolate only the AOD -mediated SW changes:

$$\Delta SW_{AOD} = \Delta SW - \Delta SW_T \quad (5)$$

200 where here ΔSW can represent either the overall SW change or the individual APRP
 201 components.

202 Aerosol-mediated SW changes differ strongly between SSPs. For example, the AOD-
 203 mediated change in cloudy sky TOA SW ($\Delta C_{AOD}/\Delta T$) is $\sim 0.7 \pm 0.1 \text{ W m}^{-2} \text{ K}^{-1}$ in SSP1-
 204 2.6, which has deep and rapid aerosol reductions (Fig. 4a), but is close to zero for those
 205 SSPs with little or no cleanup (SSP3-7.0 and SSP5-8.5). We anticipate that aerosol ra-
 206 diative forcing from aerosol-radiation interactions is likely to partly scale with overall
 207 aerosol loading, yet the AOD dependence of the non-cloudy sky APRP component ($\Delta N_{AOD}/\Delta T$)
 208 is close to zero *for all SSPs* (rightmost purple hatched bars in Fig. 4). Below, we demon-
 209 strate that near-complete cancellation between changes in scattering and absorbing aerosol
 210 are responsible for $\Delta N_{AOD} \sim 0$.

211 To gain further insights into processes controlling ΔSW , we present the regressions
 212 of the cloudy and clear APRP components (ΔC and ΔN) in Fig. 5 and Fig. 6 respec-
 213 tively. The equivalent figure for surface albedo changes is provided in Fig. S1 but is not
 214 discussed further as ΔS sensitivity to aerosol is negligible. It is striking that almost all
 215 of the cloudy sky scattering (ΔC_{scat} , grey bars) variability across SSPs can be explained
 216 by ΔAOD , whereas cloud amount changes (ΔC_{amt} , teal bars) are almost all explained
 217 by ΔT (Fig. 5). Changes in cloudy sky absorption (ΔC_{abs} , sky blue bars) are much smaller

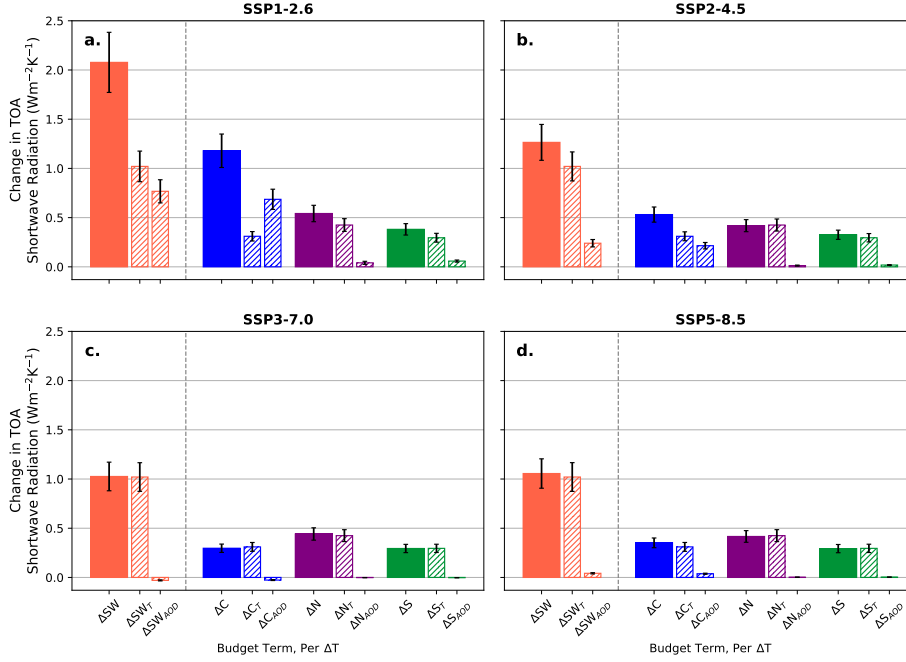


Figure 4. As in Fig. 2 but showing APRP component contributions to TOA SW changes over the 21st century that are associated with changes in ΔAOD and ΔT . Note that the TOA SW changes are normalized by ΔT here, so that T -mediated sensitivities are identical across all SSPs.

218 than those in either scattering or cloud amount and are more associated with ΔT than
 219 ΔAOD . We interpret the T -driven cloud amount decreases ($\Delta C_{amt,T}$) as the expected
 220 positive cloud feedback to warming temperatures, and the AOD -driven decreases in cloudy
 221 sky scattering ($\Delta C_{scat,AOD}$) as radiative forcing from a combination of the Twomey ef-
 222 fect and adjustments in liquid water. The positive SW cloud feedback of $\sim 0.35 \pm 0.05 \text{ W m}^{-2} \text{ K}^{-1}$
 223 over this period ($\Delta C_{amt,T}$, first hatched teal bar in all Fig. 5 panels) is consistent with
 224 cloud feedback estimates determined from observations (Sherwood et al., 2020) and from
 225 CMIP6 models (Zelinka et al., 2020). Given that we are using a very different approach
 226 for determining model cloud feedbacks from those typically used (i.e., abrupt $4 \times \text{CO}_2$ sim-
 227 ulations), this excellent agreement provides confidence in our APRP methodology for
 228 isolating cloud changes due to aerosol from those due to warming.

229 The lack of an aerosol signature in the non-cloudy sky SW changes (i.e., $\Delta N_{AOD} \sim 0$
 230 in Fig. 4) occurs despite significant changes in aerosol in the different SSPs. We further
 231 separate ΔN into scattering and absorbing components in Fig. 6 to understand this be-
 232 havior. Both ΔN_{scat} and ΔN_{abs} are strongly associated with ΔAOD (pink and peach
 233 hatched bars in Fig. 4) but the two effects almost exactly cancel each other. Because scat-
 234 tering components (primarily sulfate and organic carbon) and absorbing components (pri-
 235 marily black carbon) are often co-emitted, aerosol cleanup policies typically result in re-
 236 ductions in both scattering and *and* absorbing components. A high degree of cancella-
 237 tion was also noted in (Bond et al., 2013). Finally, we note that $\Delta N_{abs,T} \sim 0.5 \text{ W m}^{-2} \text{ K}^{-1}$.
 238 This can be attributed to increasing SW absorption by water vapor in a warmed climate
 239 (e.g., Pendergrass & Hartmann, 2013; I. L. McCoy et al., 2022).

240 The small ΔN_{AOD} indicates negligible overall SW radiative forcing from aerosol-
 241 radiation interactions. This means the vast majority of aerosol SW radiative forcing in
 242 the CMIP6 models is cloud-mediated, driven by changes in cloud scattering rather than

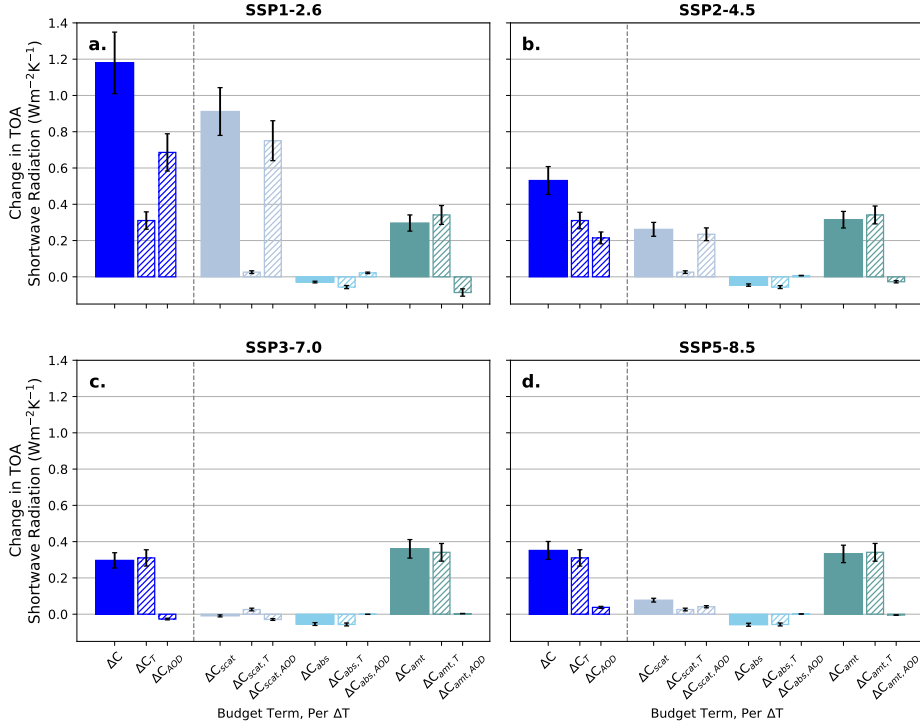


Figure 5. As in Fig. 2, but for the breakdown of cloudy sky SW changes ΔC (solid blue bar at left) into scattering (solid gray), absorption (solid sky blue), and cloud amount (solid teal) components. Each component is regressed against ΔT and ΔAOD and those dependencies are provided, respectively, in the hatched bars to the right of the solid bars.

243 changes in cloud amount. The overall SW aerosol effective radiative forcing (ERF) is the
 244 sum of ERF for aerosol-cloud interactions plus aerosol-radiation interactions, i.e., $ERF_{aer} = ERF_{aci} + ERF_{ari}$,
 245 and is determined as the sum of the AOD dependencies of the individual APRP com-
 246 ponents:

$$ERF_{aer} = ERF_{aci} + ERF_{ari} = \Delta SW_{AOD} \approx \Delta C_{AOD} + \Delta N_{AOD} + \Delta S_{AOD} \quad (6)$$

247 We use the sum of the three AOD regressions of the separate contributing terms (i.e.,
 248 ΔC_{AOD} , ΔN_{AOD} , and ΔS_{AOD}) as our estimate of SW ERF_{aer} . A multiple regression
 249 of the sum of the terms, i.e., ΔSW , against T and AOD, leads to an estimate of SW ERF_{aer}
 250 that is only 2% different. Based on our findings that ΔN_{AOD} and ΔS_{AOD} are both close
 251 to zero, $ERF_{aci} + ERF_{ari} \approx ERF_{aci} \approx \Delta C_{AOD} \approx \Delta C_{scat,AOD}$. Thus, practically all of
 252 the SW ERF_{aer} over the 21st century can be attributed to cloud scattering changes (i.e.,
 253 the Twomey effect and liquid water path adjustments). The dominant contribution of
 254 ERF_{aci} to ERF_{aer} is consistent with behavior for the 20th century (Zelinka et al., 2023).

3 Aerosol effective radiative forcing in the SSPs

255
 256 The SW ERF_{aer} determined using the APRP-regression approach described in sec-
 257 tion 2.2 is shown as a time series in Fig. 7 in preparation for comparing to ERF_{aer} es-
 258 timates from the literature. As part of the ScenarioMIP project, multi-model mean time
 259 series of net (SW+LW) ERF_{aci} and ERF_{ari} are generated using an emulation-based cal-
 260 ibration technique (Meinshausen et al., 2011; Lund et al., 2019) applied to 17 CMIP6

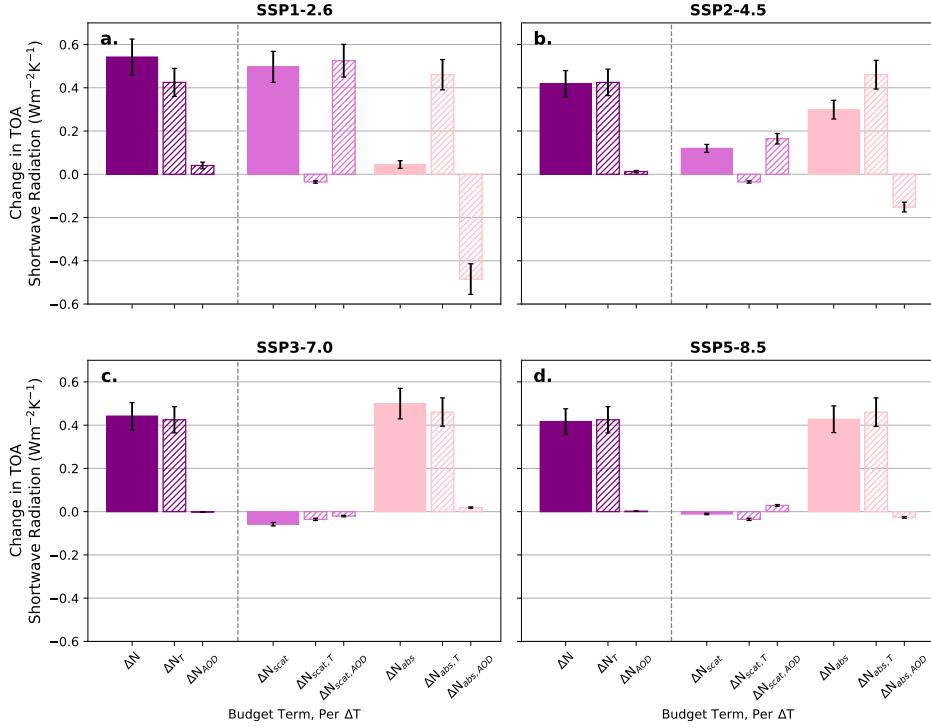


Figure 6. As in Fig. 2, but for the breakdown of non-cloudy sky SW changes ΔN (solid purple bar at left) into scattering (solid pink) and absorption (solid peach) components. Each component is regressed against ΔT and ΔAOD and those dependencies are provided, respectively, in the hatched bars to the right of the solid bars.

261 models (Leach et al., 2021). These annual mean effective radiative forcing time series
 262 from the SSPs are taken from tables provided in Smith et al. (2020), henceforth S20. We
 263 subtract the 2015-2025 mean so that the ERF_{aer} is relative to the 2020 baseline rather
 264 than to the preindustrial.

265 It is important to note that our APRP-regression approach does not provide an
 266 estimate of LW ERF_{aer} , which is necessary for comparing to the S20 net ERF_{aer} . To
 267 make an assessment of the LW aerosol radiative forcing over the 21st century, we adopt
 268 an alternative regression technique. The multimodel ensemble change in TOA net LW
 269 radiation (ΔLW) is the sum of changes due to WMGHG radiative forcing agents active
 270 in the LW (ΔLW_{WMGHG}), a temperature-dependent response (ΔLW_T) due to warm-
 271 ing temperatures and changing water vapor, and a component ΔLW_{AOD} representing
 272 aerosol-induced TOA LW changes:

$$\Delta LW = \Delta F_{WMGHG} + \Delta LW_{AOD} + \Delta LW_T \quad (7)$$

273 The radiative forcing time series ΔF_{WMGHG} is taken from S20 and includes CO_2 , CH_4 ,
 274 N_2O , and other well-mixed greenhouse gases. These are removed from ΔLW , after which
 275 the AOD and T dependent components (ΔLW_{AOD} and ΔLW_T respectively) are deter-
 276 mined using multiple linear regression against ΔAOD and ΔT .

277 Fig. 7 shows that accounting for the net (SW+LW) estimated aerosol radiative forc-
 278 ing from this study instead of only the SW ERF_{aer} *increases* the aerosol forcing discrep-
 279 ancy between S20 and our estimation by approximately 25%. This is consistent with ex-
 280 pectations that LW ERF_{aer} will be the opposite sign to the SW ERF_{aer} . Consider the
 281 radiative forcing from a negative cloud LWP adjustment, which is a typical GCM response

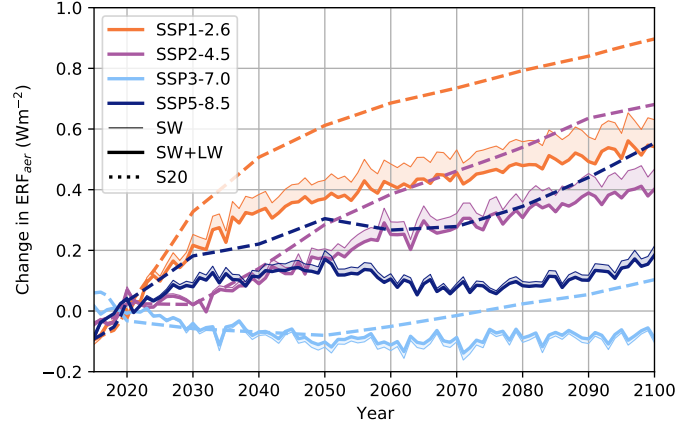


Figure 7. Time series of aerosol effective radiative forcing (ERF_{aer}) from the APRP method described in this work (solid lines) and from the CMIP6 multi-model ensemble emulation method of Smith et al. (2020) (dotted lines). All forcings are shown relative to a 2020 (2015-2025) baseline

282 to decreasing aerosol (Bellouin et al., 2020). In the SW, this decreases sunlight reflection
 283 (positive forcing), but will increase the overall LW emission because the underlying
 284 surface is warmer than the clouds above (negative forcing). Zelinka et al. (2023) as-
 285 sesses a LW ERF of 0.16 W m^{-2} ($\pm 0.34 \text{ W m}^{-2}$) for the present day (2014) minus the
 286 preindustrial in CMIP6 models. In that study the multimodel SW ERF_{aer} is -1.25 W m^{-2} .
 287 If the 21st century LW ERF_{aer} scales similarly with the SW ERF_{aer} , then for a SW ERF_{aer}
 288 of 0.6 W m^{-2} (the approximate SW forcing from 2020 to 2100 in SSP1-2.6, Fig. 7) the
 289 LW forcing would be approximately -0.08 W m^{-2} . This is very close to the -0.06 W m^{-2}
 290 we deduce from the regression analysis described above. We note that these LW ERF_{aer}
 291 estimates have large relative uncertainty ($>100\%$) but have small absolute magnitude.

292 The APRP-derived and S20 ERF_{aer} series for each SSP exhibit similar curves but
 293 with an offset between their values that increases approximately linearly with time (Fig. 7).
 294 We find that the S20 forcing increases over the 21st century are approximately $0.20\text{-}0.35 \text{ W m}^{-2}$
 295 larger than those from the APRP approach. By 2090-2100, SSP1-2.6 ERF_{aer} values are
 296 0.87 W m^{-2} (S20) and 0.61 W m^{-2} (APRP) which is equivalent to a $\sim 40\%$ difference
 297 in relative terms.

298 There are two possible reasons that may help to explain why ERF_{aer} from S20 in-
 299 creases more rapidly than from the APRP approach used in this study. Both relate to
 300 the model calibration for S20. First, it is important to note that the suite of models used
 301 here and in S20 is not identical. Although many of the CMIP6 models used in the APRP
 302 analysis are the same models as used in S20, and others are close variants of those used
 303 in S20, there are a few models in each suite that are not present in the other. Our ap-
 304 proach does not enable a harmonization of the models used. A second source of possi-
 305 ble discrepancy is that the S20 ERF_{aer} is derived from model simulations covering the
 306 historical record, and specifically comparing the year 2014 with a preindustrial (PI) con-
 307 trol (Smith et al., 2020). The model calibration parameters are then applied to model
 308 output data over the 21st century. However, as noted in the introduction, model exper-
 309 imentation has demonstrated that changing the geographic distribution of aerosol-impacting
 310 emissions can result in a different radiative forcing for the same total magnitude of emis-
 311 sions (Persad & Caldeira, 2018).

312 To investigate these potential reasons in more detail, we first note that the multi-
 313 model mean ERF_{aer} (LW+SW) for 2014 minus the PI from S20 is -1.01 W m^{-2} with
 314 a standard deviation of 0.23 W m^{-2} . Zelinka et al. (2023) applied the APRP method
 315 to historical simulations (2014 minus PI) with a similar model suite as we use for the 21st
 316 century and obtained an estimate of ERF_{aer} for the same period as S20 (2014 minus the
 317 PI) of -1.09 W m^{-2} with a standard deviation of 0.24 W m^{-2} . The similarity in the mul-
 318 timodel forcing mean and spread between these two studies provides some confidence that
 319 different model selection between the approaches in S20 and our study is probably *not*
 320 responsible for the forcing differences in Fig. 7 as they are examined relative to their re-
 321 spective baselines.

322 To investigate the possibility that changes in the *location* of the key emission re-
 323 gions may be responsible for some of the ERF_{aer} discrepancy between the S20 and our
 324 APRP estimates (Fig. 7), we introduce a metric that is sensitive to a geographic shift
 325 of major emission regions in the present day (2015-2025) and the later part of the 21st
 326 century. One can argue that the rise of emissions in SE Asia occurred prior to 2014 and
 327 so these emissions are well-reflected in the model calibration used in S20. On the other
 328 hand, the 21st century is likely to see a shift in the main anthropogenic emission regions
 329 as cleanup policies start to take effect in East Asia while the emissions in rapidly-industrializing
 330 Africa may remain relatively flat (Turnock et al., 2020). We find that the difference in
 331 AOD between a large region of East Asia ($0-45^\circ\text{N}$, $60-130^\circ\text{E}$) and Equatorial Africa (15°S -
 332 15°N , 30°W - 30°E), i.e., $AOD_{Africa} - AOD_{Asia}$, explains just over 80% of the variance in
 333 the S20-APRP discrepancy in ERF_{aer} (Fig. 8). It seems reasonable to postulate that much
 334 of the discrepancy between the APRP and S20 estimates of ERF_{aer} over the 21st cen-
 335 tury can likely be attributed to shifting emission locations. Thus, it is important that
 336 future work explores how different emission locations may impact not only regional tem-
 337 perature responses but also the global mean response. For the 21st century temperature
 338 responses (section 4), we will use both forcing estimates in our calculations, with differ-
 339 ences between the two providing a measure of the impact of aerosol forcing uncertainty
 340 on future warming.

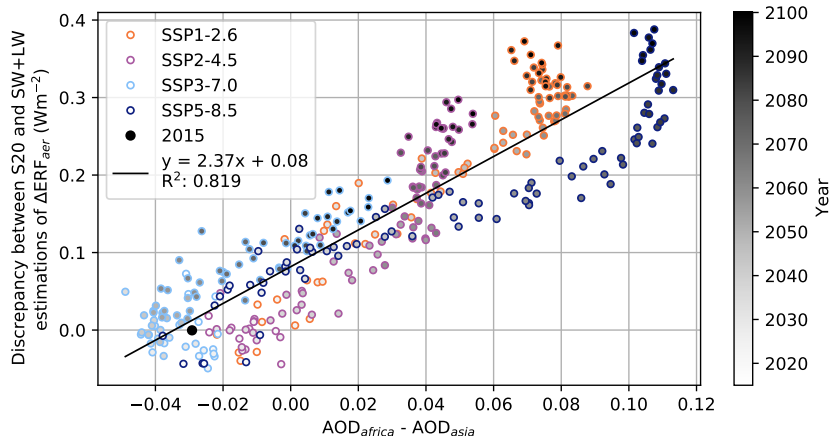


Figure 8. Difference between the S20 and APRP-derived ERF_{aer} regressed against the difference in AOD between a region in Equatorial Africa and East Asia (see text). The symbol shading indicates the year (see bar at right), with the initial value (2015) shown with the solid circle.

4 Temperature responses

For each of the four SSPs, the ERF_{aer} time series using the APRP method (Fig. 7) are used together with all other anthropogenic radiative forcings (taken from Smith et al. (2020)) to estimate a future global mean surface air temperature time series projection. As motivated in the introduction, we decouple future changes in aerosol from future changes in all other anthropogenic forcings (predominantly WMGHGs). This is achieved by considering the 16 potential combinations of aerosol forcing (ERF_{aer}) from one of the four SSPs with all other anthropogenic forcings (ERF_{other}) taken from another SSP. In this way, we can consider the effect of different aerosol cleanup strategies on scenarios that involve different levels of decarbonization. For example, we can examine the effects of rapid aerosol cleanup on a future with very limited decarbonization by pairing the future aerosol forcing from SSP1-2.6 with other anthropogenic aerosol forcings taken from SSP5-8.5.

Global annual mean temperature time series from 1750 to 2100 are calculated using the simple two-layer climate model used in Dvorak et al. (2022) and a very similar approach to Geoffroy et al. (2013). For each of 100,000 ensemble members, model parameters are drawn randomly from normal distributions as specified in Dvorak et al. (2022), with the same truncation of the deep ocean heat capacity to avoid very small values. Instead of using a uniform distribution of equilibrium climate sensitivity (ECS) as in Dvorak et al. (2022), we draw from a normal distribution for the climate feedback parameter with mean and standard deviation of $1.20 \text{ W m}^{-2} \text{ K}^{-1}$ and $0.26 \text{ W m}^{-2} \text{ K}^{-1}$, respectively. This gives a 50th percentile ECS value of 3.1 K, with 5th and 95th percentiles of 2.3 and 4.8, respectively, which are very close to those assessed in Sherwood et al. (2020). Radiative forcings and resulting temperatures are all taken relative to 2020 values.

An example showing input radiative forcings and output decadal mean temperature responses is shown in Fig. 9. In this case, ERF_{aer} is taken from SSP1-2.6 which experiences a deep and rapid decrease in aerosol forcing magnitude from the present day out to ~ 2040 (also see Fig. 7). The other, non-aerosol radiative forcings for this example are taken from SSP2-4.5. The ramp-up in aerosol forcing magnitude over the second half of the 20th century is followed by cleanup over the early 21st century, leading to a 50-year delay in global warming (Fig. 9b). Warming rates over the period 2020-2050 are 20-40% greater with aerosol cleanup than without. This highlights the critically important contribution of aerosol cleanup to near-term warming rates.

Fig. S2 compares global mean temperature time series taken from the 18 member ScenarioMIP CMIP6 global model ensemble with those from the simple climate model. For each of the four SSPs, the simple climate model projected median temperature increase agrees very well with the CMIP6 multimodel mean, providing confidence in the simple climate model projections.

Cumulative probability distributions of projected global mean surface air temperature warming rates over the three decade period 2020-2050 are shown in Fig. 10 for different combinations of ERF_{aer} and ERF_{other} taken from the SSPs. The global mean temperature in 2020 is approximately +1.2 C above the preindustrial (Morice et al., 2021). Given this, additional warming of 0.8 C over the period 2020-2050 (a mean warming rate of $0.27 \text{ C decade}^{-1}$) would lead to a global mean surface air temperature that reaches 2 C above the preindustrial, a threshold that nations have pledged not to exceed as part of the 2015 Paris Climate Agreement. Climate change risks increase dramatically if the 2 C threshold is surpassed (Pörtner et al., 2022).

Possible aerosol cleanup pathways over 2020-2050 have significant impacts on warming rates over that period (Fig. 10). For example, with strong mitigation of carbon emissions (ERF_{other} from SSP1-2.6), slow (purple) or no (blue) aerosol cleanup likely leads to temperatures that remain below 2C by 2050 (Fig. 10a). However, even with strong

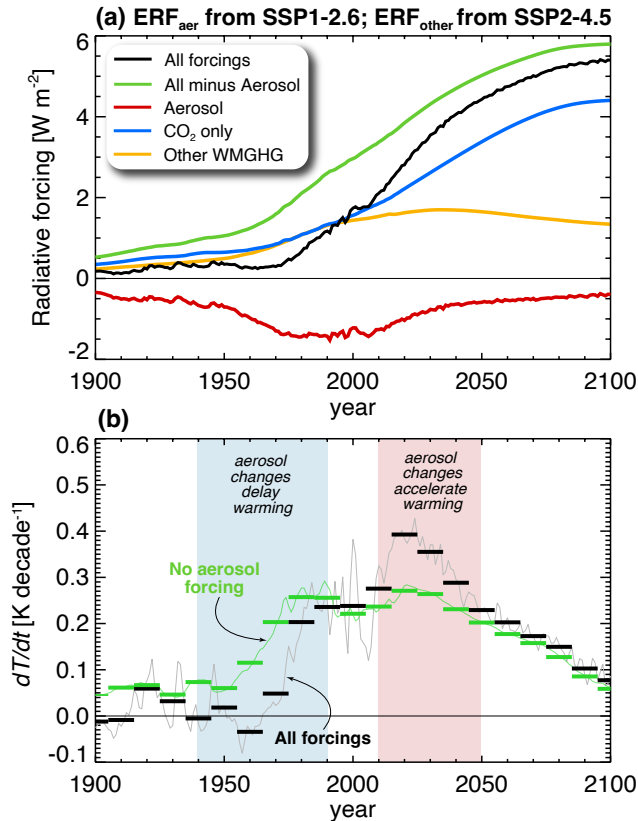


Figure 9. Example of (a) radiative forcings, and (b) predicted decadal temperature trends from the simple two-layer climate model. The model is run with all forcings (black) and with all forcings except the aerosol radiative forcing (green). In this case, the aerosol forcing series is taken from our APRP method applied to SSP1-2.6 (see Fig. 7). The non-aerosol (other) forcings are taken from SSP2-4.5. In (a), the greenhouse forcing is broken down into that from CO₂ (blue) and from other WMGHGs (orange), which together account for almost all of the non-aerosol radiative forcing (green). Panel (b) shows the annual warming rate (thin lines) and the decadal mean warming rates (horizontal bars). Aerosol increases during the period from ~1940 to ~1990 dramatically reduced the warming over that period, whereas from 2010-2050 the deep and rapid cleanup associated with the SSP1-2.6 future aerosol trend leads to a considerable acceleration of the warming.

392 decarbonization commitments, deep and rapid aerosol cleanup results in a 5% chance
 393 (APRP) to a 12% chance (S20) of reaching 2C by 2050 (orange curves).

394 Given current, nationally-determined contributions to decarbonization, it is unlikely
 395 that greenhouse gas radiative forcing will follow the specifications of SSP1-2.6 and will
 396 more likely track those in SSP2-4.5 (Liu & Raftery, 2021). In this case, aerosol cleanup
 397 choices profoundly impact the probability of remaining below 2C by 2050 (Fig. 10b). With
 398 (ERF_{other} from SSP2-4.5, aggressive aerosol cleanup (orange curves, ERF_{aer} from SSP1-
 399 2.6) more than doubles the probability of reaching 2C by 2050 from 20-30% (blue curves)
 400 to over 75% (Fig. 10b). This range indicates that aerosol cleanup choices over the next
 401 few decades can make the difference between achieving a 2C target and missing it. It
 402 is likely that both of the unmitigated carbon emission scenarios SSP3-7.0 and SSP5-8.5

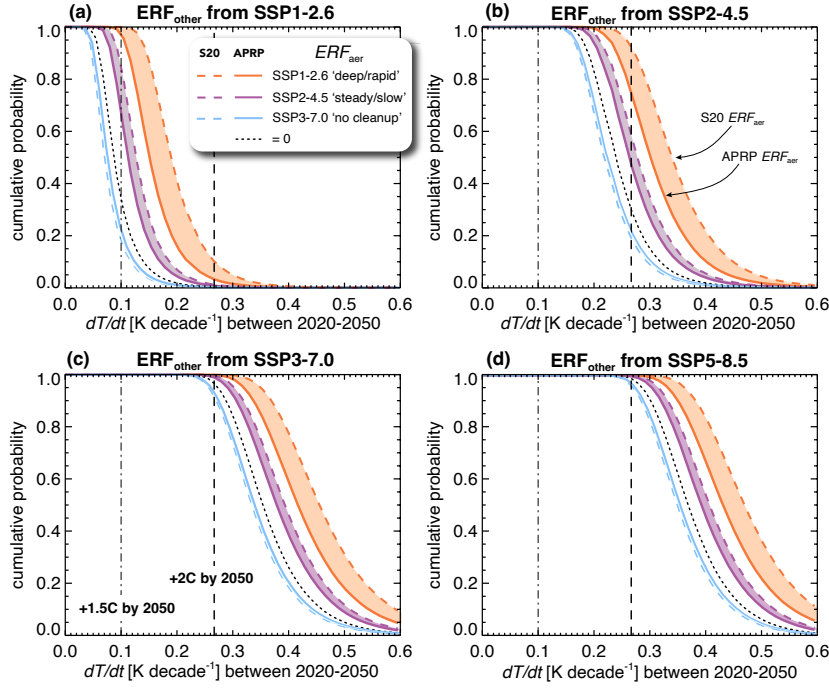


Figure 10. Probability that the global mean surface decadal warming rate over the period 2020-2050 will exceed the value on the abscissa. Temperature is calculated from the ensemble of simple climate models described in Section 4. Different line colors within each panel represent different aerosol pathways: deep and rapid (orange, SSP1-2.6), steady and slow (purple, SSP2-4.5), no cleanup (light blue, SSP3-7.0), and a case with exactly zero aerosol forcing (dotted line, $ERF_{aer}=0$). Each panel presents a different pathway for the other anthropogenic forcings: (a) SSP1-2.6, (b) SSP2-4.5, (c) SSP3-7.0, and (d) SSP5-8.5. The solid and dashed lines for each aerosol pathway represent the ERF_{aer} taken from the APRP method and from S20 respectively, and so the shaded regions represent uncertainty in the aerosol forcing estimate used. Results with aerosol from the SSP5-8.5 scenario are almost identical to those from the SSP3-7.0 scenario, so are omitted. Vertical lines indicate the warming rates required to reach 2C (dashed) and 1.5 C (dash-dot) above preindustrial levels by 2050.

403
404

will exceed 2C by 2050, although aggressive aerosol mitigation makes this outcome almost a certainty.

405
406
407
408
409
410
411
412

As explored in section 3, the APRP method produces a weaker increase in ERF_{aer} than for S20, which likely stems from the shifting geographic location of the aerosol emissions. Thus, regional shifts in aerosol emission locations over the 21st century may be somewhat buffering the overall effects of aerosol cleanup. These regional shifts appear to have a significant impact on global warming rates in addition to any local effects that are induced. This result is consistent with (Persad & Caldeira, 2018) and strongly warrants a concerted effort to better constrain future aerosol forcing changes (Persad et al., 2022).

5 Discussion and Conclusions

The results presented here demonstrate that global warming rates over the next few decades (2020-2050) will be altered significantly by air quality policies designed to reduce the negative health consequences of particulate matter. There are major uncertainties in aerosol radiative forcing, so the consequences of aerosol cleanup policies on climate could potentially be relatively small. On the other hand, the rapid cleanup of particulate-forming emissions that began in the early 2000s may control the success or failure of the 2015 Paris Climate Agreement to restrict global mean surface air temperatures to no more than 2C above the preindustrial. Thus, it is imperative that aerosols be included in climate risk assessments.

Our findings are broadly consistent with the analysis of (Watson-Parris & Smith, 2022), wherein the effects of different assumptions about how uncertainty in how effective aerosol radiative forcing will change over the coming decades were found to influence whether climate warming targets may be met. A novel aspect of our study is that we show that shifts in the location of aerosol emissions over the coming decades may also have an important influence on the magnitude of global warming due to aerosol cleanup policies. Shifting emission locations in the coming decades likely renders the relationship between global emissions and ERF_{aer} somewhat nonlinear, motivating further studies on the connection between emission locations and the susceptibility of downwind cloud fields in order to better project how future, changing aerosol and precursor emissions project onto global warming (Persad & Caldeira, 2018; Wilcox et al., 2023). Our results suggest that 21st century changes in emission locations may somewhat reduce the probability of exceeding the 2C target compared to a world where emission locations do not change. However, there are still significant questions about which countries will adopt stringent cleanup policies and which may not, so that future aerosol emission strengths and locations may be different from those represented in the CMIP6 ScenarioMIP SSPs.

In the CMIP6 models, we find that most of the aerosol radiative forcing change in coming decades is driven by radiative forcing from aerosol-cloud interactions. There is increasing focus in recent years on the idea of deliberately introducing aerosol particles into marine clouds with the view of increasing their reflection of sunlight to cool the Earth. This possible climate intervention strategy, known as *marine cloud brightening* (Latham et al., 2012; Wood, 2021), aims to produce a negative ERF_{aer} from aerosol-cloud interactions in marine low clouds. The climate efficacy of marine cloud brightening is currently not well understood (e.g., Stjern et al., 2018) and there are no existing protocols for incorporating marine cloud brightening into the SSP approach. Given the importance of emission location shown in this study, efforts to develop realistic climate intervention scenarios are important, in particular for marine cloud brightening whose emission geography would be very different from that due to changing anthropogenic activities.

6 Open Research

All CMIP6 ScenarioMIP simulations used in this study are available at <https://esgf-node.llnl.gov/projects/cmip6/>. For the APRP analysis, we use the code available from Mark Zelinka. (2021). *mzelinka/aprp*: Sep 17, 2021 Release (v1.0). Zenodo. <https://doi.org/10.5281/zenodo.55141>

Acknowledgments

The authors thank Dargan Frierson for helping to identify and download CMIP6 data used in this study, and for providing useful guidance on the use of the simple climate model. We also thank Geeta Persad for insightful discussions and acknowledge the World Climate Research Programme and its Working Group on Coupled Modelling for coordinating CMIP6; the climate modeling groups involved for their simulations; the Earth System Grid Federation (ESGF) for archiving and facilitating data usage; and the multi-

462 ple funding agencies who support CMIP and ESGF efforts. Research by ILM was sup-
 463 ported by the NOAA Climate and Global Change Postdoctoral Fellowship Program, ad-
 464 ministered by UCAR's Cooperative Programs for the Advancement of Earth System Sci-
 465 ence (CPAESS) under award NA18NWS4620043B and the NOAA cooperative agreements
 466 NA17OAR4320101 and NA22OAR4320151. MAV and RW were funded on indirect cost
 467 recovery support from grants to UW. We thank our editor, [], and [] anonymous review-
 468 ers for their insights and suggestions for improving our manuscript.

469 References

- 470 Bellouin, N., Quaas, J., Gryspeerdt, E., Kinne, S., Stier, P., Watson-
 471 Parris, D., ... Stevens, B. (2020). Bounding Global Aerosol Ra-
 472 diative Forcing of Climate Change. *Reviews of Geophysics*, 58(1),
 473 e2019RG000660. Retrieved 2020-10-06, from [https://agupubs](https://agupubs.onlinelibrary.wiley.com/doi/abs/10.1029/2019RG000660)
 474 [.onlinelibrary.wiley.com/doi/abs/10.1029/2019RG000660](https://agupubs.onlinelibrary.wiley.com/doi/abs/10.1029/2019RG000660) (_eprint:
 475 <https://agupubs.onlinelibrary.wiley.com/doi/pdf/10.1029/2019RG000660>) doi:
 476 10.1029/2019RG000660
- 477 Bond, T. C., Doherty, S. J., Fahey, D. W., Forster, P. M., Berntsen, T., DeAngelo,
 478 B. J., ... Zender, C. S. (2013, June). Bounding the role of black carbon in
 479 the climate system: A scientific assessment: BLACK CARBON IN THE CLI-
 480 MATE SYSTEM. *Journal of Geophysical Research: Atmospheres*, 118(11),
 481 5380–5552. Retrieved 2014-06-01, from [http://doi.wiley.com/10.1002/](http://doi.wiley.com/10.1002/jgrd.50171)
 482 [jgrd.50171](http://doi.wiley.com/10.1002/jgrd.50171) doi: 10.1002/jgrd.50171
- 483 Cao, Y., Zhu, Y., Wang, M., Rosenfeld, D., Liang, Y., Liu, J., ... Bai, H. (2023).
 484 Emission Reductions Significantly Reduce the Hemispheric Contrast in Cloud
 485 Droplet Number Concentration in Recent Two Decades. *Journal of Geophys-*
 486 *ical Research: Atmospheres*, 128(2), e2022JD037417. Retrieved 2023-02-02,
 487 from <https://onlinelibrary.wiley.com/doi/abs/10.1029/2022JD037417>
 488 (_eprint: <https://onlinelibrary.wiley.com/doi/pdf/10.1029/2022JD037417>) doi:
 489 10.1029/2022JD037417
- 490 Colman, R. A., & McAvaney, B. J. (1997). A study of general circula-
 491 tion model climate feedbacks determined from perturbed sea surface
 492 temperature experiments. *Journal of Geophysical Research: Atmo-*
 493 *spheres*, 102(D16), 19383–19402. Retrieved 2023-06-09, from [https://](https://onlinelibrary.wiley.com/doi/abs/10.1029/97JD00206)
 494 onlinelibrary.wiley.com/doi/abs/10.1029/97JD00206 (_eprint:
 495 <https://onlinelibrary.wiley.com/doi/pdf/10.1029/97JD00206>) doi: 10.1029/
 496 97JD00206
- 497 Dvorak, M. T., Armour, K. C., Frierson, D. M. W., Proistosescu, C., Baker, M. B.,
 498 & Smith, C. J. (2022, June). Estimating the timing of geophysical commit-
 499 ment to 1.5 and 2.0 °C of global warming. *Nature Climate Change*, 12(6),
 500 547–552. Retrieved 2022-07-07, from [https://www.nature.com/articles/](https://www.nature.com/articles/s41558-022-01372-y)
 501 [s41558-022-01372-y](https://www.nature.com/articles/s41558-022-01372-y) (Number: 6 Publisher: Nature Publishing Group) doi:
 502 10.1038/s41558-022-01372-y
- 503 Eyring, V., Bony, S., Meehl, G. A., Senior, C. A., Stevens, B., Stouffer, R. J., &
 504 Taylor, K. E. (2016, May). Overview of the Coupled Model Intercomparison
 505 Project Phase 6 (CMIP6) experimental design and organization. *Geosci-*
 506 *entific Model Development*, 9(5), 1937–1958. Retrieved 2023-06-07, from
 507 <https://gmd.copernicus.org/articles/9/1937/2016/> (Publisher: Coperni-
 508 cus GmbH) doi: 10.5194/gmd-9-1937-2016
- 509 Feng, L., Smith, S. J., Braun, C., Crippa, M., Gidden, M. J., Hoesly, R., ... van der
 510 Werf, G. R. (2019, August). Gridded Emissions for CMIP6. *Geosci-*
 511 *entific Model Development Discussions*, 1–25. Retrieved 2019-11-15, from
 512 <https://www.geosci-model-dev-discuss.net/gmd-2019-195/> doi:
 513 10.5194/gmd-2019-195
- 514 Geoffroy, O., Saint-Martin, D., Olivié, D. J. L., Voldoire, A., Bellon, G., & Tytéca,

- 515 S. (2013, March). Transient Climate Response in a Two-Layer Energy-Balance
 516 Model. Part I: Analytical Solution and Parameter Calibration Using CMIP5
 517 AOGCM Experiments. *Journal of Climate*, 26(6), 1841–1857. Retrieved
 518 2022-12-27, from [http://journals.ametsoc.org/view/journals/clim/26/](http://journals.ametsoc.org/view/journals/clim/26/6/jcli-d-12-00195.1.xml)
 519 [6/jcli-d-12-00195.1.xml](http://journals.ametsoc.org/view/journals/clim/26/6/jcli-d-12-00195.1.xml) (Publisher: American Meteorological Society
 520 Section: Journal of Climate) doi: 10.1175/JCLI-D-12-00195.1
- 521 Hansen, J., Sato, M., Ruedy, R., Nazarenko, L., Lacis, A., Schmidt, G. A.,
 522 ... Zhang, S. (2005). Efficacy of climate forcings. *Journal of Geo-*
 523 *physical Research: Atmospheres*, 110(D18). Retrieved 2023-06-07, from
 524 <https://onlinelibrary.wiley.com/doi/abs/10.1029/2005JD005776>
 525 (_eprint: <https://onlinelibrary.wiley.com/doi/pdf/10.1029/2005JD005776>)
 526 doi: 10.1029/2005JD005776
- 527 Latham, J., Bower, K., Choullarton, T., Coe, H., Connolly, P., Cooper, G., ...
 528 Wood, R. (2012, September). Marine cloud brightening. *Philosophical*
 529 *Transactions of the Royal Society A: Mathematical, Physical and Engineer-*
 530 *ing Sciences*, 370(1974), 4217–4262. Retrieved 2014-06-01, from [http://](http://rsta.royalsocietypublishing.org/cgi/doi/10.1098/rsta.2012.0086)
 531 rsta.royalsocietypublishing.org/cgi/doi/10.1098/rsta.2012.0086
 532 doi: 10.1098/rsta.2012.0086
- 533 Leach, N. J., Jenkins, S., Nicholls, Z., Smith, C. J., Lynch, J., Cain, M., ...
 534 Allen, M. R. (2021, May). FaIRv2.0.0: a generalized impulse response
 535 model for climate uncertainty and future scenario exploration. *Geoscientific*
 536 *Model Development*, 14(5), 3007–3036. Retrieved 2023-06-15, from
 537 <https://gmd.copernicus.org/articles/14/3007/2021/> (Publisher: Coper-
 538 nicus GmbH) doi: 10.5194/gmd-14-3007-2021
- 539 Liu, P. R., & Raftery, A. E. (2021, February). Country-based rate of emissions
 540 reductions should increase by 80% beyond nationally determined contribu-
 541 tions to meet the 2 °C target. *Communications Earth & Environment*, 2(1),
 542 1–10. Retrieved 2023-09-26, from [https://www.nature.com/articles/](https://www.nature.com/articles/s43247-021-00097-8)
 543 [s43247-021-00097-8](https://www.nature.com/articles/s43247-021-00097-8) (Number: 1 Publisher: Nature Publishing Group) doi:
 544 10.1038/s43247-021-00097-8
- 545 Lund, M. T., Myhre, G., & Samset, B. H. (2019, November). Anthropogenic
 546 aerosol forcing under the Shared Socioeconomic Pathways. *Atmospheric*
 547 *Chemistry and Physics*, 19(22), 13827–13839. Retrieved 2023-02-23, from
 548 <https://acp.copernicus.org/articles/19/13827/2019/> (Publisher:
 549 Copernicus GmbH) doi: 10.5194/acp-19-13827-2019
- 550 Masson-Delmotte, V., et al. (Eds.). (2021). *Climate Change 2021: The Phys-*
 551 *ical Science Basis. Contribution of Working Group I to the Sixth Assess-*
 552 *ment Report of the Intergovernmental Panel on Climate Change.* Cambridge,
 553 United Kingdom and New York, NY, USA: Cambridge University Press. doi:
 554 10.1017/9781009157896
- 555 McCoy, D. T., Bender, F. A.-M., Grosvenor, D. P., Mohrmann, J. K., Hartmann,
 556 D. L., Wood, R., & Field, P. R. (2018, February). Predicting decadal
 557 trends in cloud droplet number concentration using reanalysis and satellite
 558 data. *Atmospheric Chemistry and Physics*, 18(3), 2035–2047. Retrieved
 559 2019-05-27, from <https://www.atmos-chem-phys.net/18/2035/2018/> doi:
 560 <https://doi.org/10.5194/acp-18-2035-2018>
- 561 McCoy, I. L., Vogt, M. A., & Wood, R. (2022). Absorbing Aerosol Choices In-
 562 fluences Precipitation Changes Across Future Scenarios. *Geophysical Re-*
 563 *search Letters*, 49(8), e2022GL097717. Retrieved 2022-04-16, from [http://](http://onlinelibrary.wiley.com/doi/abs/10.1029/2022GL097717)
 564 onlinelibrary.wiley.com/doi/abs/10.1029/2022GL097717 (_eprint:
 565 <https://agupubs.onlinelibrary.wiley.com/doi/pdf/10.1029/2022GL097717>) doi:
 566 10.1029/2022GL097717
- 567 Meehl, G. A., Washington, W. M., Ammann, C. M., Arblaster, J. M., Wigley,
 568 T. M. L., & Tebaldi, C. (2004, October). Combinations of Natural and
 569 Anthropogenic Forcings in Twentieth-Century Climate. *Journal of Climate*,

- 570 17(19), 3721–3727. Retrieved 2023-06-07, from https://journals.ametsoc.org/view/journals/clim/17/19/1520-0442.2004.017_3721_conaaf_2.0.co_2.xml (Publisher: American Meteorological Society Section: Journal of Climate) doi: 10.1175/1520-0442(2004)017(3721:CONAAF)2.0.CO;2
- 571
572
573
- 574 Meinshausen, M., Raper, S. C. B., & Wigley, T. M. L. (2011, February). Emulating coupled atmosphere-ocean and carbon cycle models with a simpler model, MAGICC6 – Part 1: Model description and calibration. *Atmospheric Chemistry and Physics*, 11(4), 1417–1456. Retrieved 2023-02-13, from <https://acp.copernicus.org/articles/11/1417/2011/> (Publisher: Copernicus GmbH) doi: 10.5194/acp-11-1417-2011
- 575
576
577
578
579
- 580 Morice, C. P., Kennedy, J. J., Rayner, N. A., Winn, J. P., Hogan, E., Killick, R. E., ... Simpson, I. R. (2021). An Updated Assessment of Near-Surface Temperature Change From 1850: The HadCRUT5 Data Set. *Journal of Geophysical Research: Atmospheres*, 126(3), e2019JD032361. Retrieved 2023-07-21, from <https://onlinelibrary.wiley.com/doi/abs/10.1029/2019JD032361> (eprint: <https://onlinelibrary.wiley.com/doi/pdf/10.1029/2019JD032361>) doi: 10.1029/2019JD032361
- 581
582
583
584
585
586
- 587 O'Neill, B. C., Tebaldi, C., van Vuuren, D. P., Eyring, V., Friedlingstein, P., Hurtt, G., ... Sanderson, B. M. (2016, September). The Scenario Model Intercomparison Project (ScenarioMIP) for CMIP6. *Geoscientific Model Development*, 9(9), 3461–3482. Retrieved 2019-11-03, from <https://www.geosci-model-dev.net/9/3461/2016/> doi: 10.5194/gmd-9-3461-2016
- 588
589
590
591
- 592 Pendergrass, A. G., & Hartmann, D. L. (2013, September). The Atmospheric Energy Constraint on Global-Mean Precipitation Change. *Journal of Climate*, 27(2), 757–768. Retrieved 2020-02-24, from <https://journals.ametsoc.org/doi/full/10.1175/JCLI-D-13-00163.1> doi: 10.1175/JCLI-D-13-00163.1
- 593
594
595
- 596 Persad, G. G., & Caldeira, K. (2018, August). Divergent global-scale temperature effects from identical aerosols emitted in different regions. *Nature Communications*, 9(1), 3289. Retrieved 2023-06-07, from <https://www.nature.com/articles/s41467-018-05838-6> (Number: 1 Publisher: Nature Publishing Group) doi: 10.1038/s41467-018-05838-6
- 597
598
599
600
- 601 Persad, G. G., Samset, B. H., & Wilcox, L. J. (2022, November). Aerosols must be included in climate risk assessments. *Nature*, 611(7937), 662–664. Retrieved 2023-06-07, from <https://www.nature.com/articles/d41586-022-03763-9> (Bandiera_abtest: a Cg-type: Comment Number: 7937 Publisher: Nature Publishing Group Subject_term: Climate change, Atmospheric science, Policy) doi: 10.1038/d41586-022-03763-9
- 602
603
604
605
606
- 607 Pörtner, H.-O., et al. (Eds.). (2022). *Climate Change 2022: Impacts, Adaptation and Vulnerability. Contribution of Working Group II to the Sixth Assessment Report of the Intergovernmental Panel on Climate Change*.
- 608
609
- 610 Qu, X., Hall, A., Klein, S. A., & DeAngelis, A. M. (2015, September). Positive tropical marine low-cloud cover feedback inferred from cloud-controlling factors. *Geophysical Research Letters*, 42(18), 2015GL065627. Retrieved 2017-11-17, from <http://onlinelibrary.wiley.com/doi/10.1002/2015GL065627/abstract> doi: 10.1002/2015GL065627
- 611
612
613
614
- 615 Quaas, J., Jia, H., Smith, C., Albright, A. L., Aas, W., Bellouin, N., ... Schulz, M. (2022, September). Robust evidence for reversal of the trend in aerosol effective climate forcing. *Atmospheric Chemistry and Physics*, 22(18), 12221–12239. Retrieved 2023-05-08, from <https://acp.copernicus.org/articles/22/12221/2022/> (Publisher: Copernicus GmbH) doi: 10.5194/acp-22-12221-2022
- 616
617
618
619
620
- 621 Riahi, K., van Vuuren, D. P., Kriegler, E., Edmonds, J., O'Neill, B. C., Fujimori, S., ... Tavoni, M. (2017, January). The Shared Socioeconomic Pathways and their energy, land use, and greenhouse gas emissions implications: An overview. *Global Environmental Change*, 42, 153–168. Retrieved 2021-
- 622
623
624

- 625 09-14, from [https://www.sciencedirect.com/science/article/pii/](https://www.sciencedirect.com/science/article/pii/S0959378016300681)
626 S0959378016300681 doi: 10.1016/j.gloenvcha.2016.05.009
- 627 Seinfeld, J. H., Bretherton, C., Carslaw, K. S., Coe, H., DeMott, P. J., Dunlea,
628 E. J., ... Wood, R. (2016, May). Improving our fundamental understand-
629 ing of the role of aerosolcloud interactions in the climate system. *Proceed-*
630 *ings of the National Academy of Sciences*, 113(21), 5781–5790. Retrieved
631 2016-05-25, from <http://www.pnas.org/content/113/21/5781> doi:
632 10.1073/pnas.1514043113
- 633 Sherwood, S. C., Webb, M. J., Annan, J. D., Armour, K. C., Forster, P. M.,
634 Hargreaves, J. C., ... Zelinka, M. D. (2020). An Assessment of Earth's
635 Climate Sensitivity Using Multiple Lines of Evidence. *Reviews of Geo-*
636 *physics*, 58(4), e2019RG000678. Retrieved 2021-10-10, from [https://](https://onlinelibrary.wiley.com/doi/abs/10.1029/2019RG000678)
637 onlinelibrary.wiley.com/doi/abs/10.1029/2019RG000678 (eprint:
638 <https://onlinelibrary.wiley.com/doi/pdf/10.1029/2019RG000678>) doi:
639 10.1029/2019RG000678
- 640 Smith, C. J., Kramer, R. J., Myhre, G., Alterskjær, K., Collins, W., Sima, A., ...
641 Forster, P. M. (2020, August). Effective radiative forcing and adjustments in
642 CMIP6 models. *Atmospheric Chemistry and Physics*, 20(16), 9591–9618. Re-
643 trieved 2021-03-17, from [https://acp.copernicus.org/articles/20/9591/](https://acp.copernicus.org/articles/20/9591/2020/)
644 [2020/](https://acp.copernicus.org/articles/20/9591/2020/) (Publisher: Copernicus GmbH) doi: 10.5194/acp-20-9591-2020
- 645 Stjern, C. W., Muri, H., Ahlm, L., Boucher, O., Cole, J. N. S., Ji, D., ...
646 Kristjánsson, J. E. (2018, January). Response to marine cloud brightening
647 in a multi-model ensemble. *Atmospheric Chemistry and Physics*, 18(2), 621–
648 634. Retrieved 2019-08-02, from [https://www.atmos-chem-phys.net/18/621/](https://www.atmos-chem-phys.net/18/621/2018/acp-18-621-2018.html)
649 [2018/acp-18-621-2018.html](https://www.atmos-chem-phys.net/18/621/2018/acp-18-621-2018.html) doi: <https://doi.org/10.5194/acp-18-621-2018>
- 650 Taylor, K. E., Crucifix, M., Braconnot, P., Hewitt, C. D., Doutriaux, C., Broccoli,
651 A. J., ... Webb, M. J. (2007, June). Estimating Shortwave Radiative Forcing
652 and Response in Climate Models. *Journal of Climate*, 20(11), 2530–2543.
653 Retrieved 2020-04-17, from [https://journals.ametsoc.org/doi/full/](https://journals.ametsoc.org/doi/full/10.1175/JCLI4143.1)
654 [10.1175/JCLI4143.1](https://journals.ametsoc.org/doi/full/10.1175/JCLI4143.1) (Publisher: American Meteorological Society) doi:
655 10.1175/JCLI4143.1
- 656 Turnock, S. T., Allen, R. J., Andrews, M., Bauer, S. E., Deushi, M., Emmons, L.,
657 ... Zhang, J. (2020, November). Historical and future changes in air pol-
658 lutants from CMIP6 models. *Atmospheric Chemistry and Physics*, 20(23),
659 14547–14579. Retrieved 2023-06-16, from [https://acp.copernicus.org/](https://acp.copernicus.org/articles/20/14547/2020/)
660 [articles/20/14547/2020/](https://acp.copernicus.org/articles/20/14547/2020/) (Publisher: Copernicus GmbH) doi: 10.5194/
661 acp-20-14547-2020
- 662 Watson-Parris, D., & Smith, C. J. (2022, December). Large uncertainty in fu-
663 ture warming due to aerosol forcing. *Nature Climate Change*, 12(12), 1111–
664 1113. Retrieved 2023-09-01, from [https://www.nature.com/articles/](https://www.nature.com/articles/s41558-022-01516-0)
665 [s41558-022-01516-0](https://www.nature.com/articles/s41558-022-01516-0) (Number: 12 Publisher: Nature Publishing Group) doi:
666 10.1038/s41558-022-01516-0
- 667 Wilcox, L. J., Allen, R. J., Samset, B. H., Bollasina, M. A., Griffiths, P. T., Keeble,
668 J., ... Westervelt, D. M. (2023, August). The Regional Aerosol Model In-
669 tercomparison Project (RAMIP). *Geoscientific Model Development*, 16(15),
670 4451–4479. Retrieved 2023-09-19, from [https://gmd.copernicus.org/](https://gmd.copernicus.org/articles/16/4451/2023/)
671 [articles/16/4451/2023/](https://gmd.copernicus.org/articles/16/4451/2023/) (Publisher: Copernicus GmbH) doi: 10.5194/
672 gmd-16-4451-2023
- 673 Wood, R. (2021, October). Assessing the potential efficacy of marine cloud
674 brightening for cooling Earth using a simple heuristic model. *Atmospheric*
675 *Chemistry and Physics*, 21(19), 14507–14533. Retrieved 2021-10-02, from
676 <https://acp.copernicus.org/articles/21/14507/2021/> (Publisher:
677 Copernicus GmbH) doi: 10.5194/acp-21-14507-2021
- 678 Zelinka, M. D., Myers, T. A., McCoy, D. T., Po-Chedley, S., Caldwell,
679 P. M., Ceppi, P., ... Taylor, K. E. (2020). Causes of Higher Cli-

680 mate Sensitivity in CMIP6 Models. *Geophysical Research Letters*,
681 47(1), e2019GL085782. Retrieved 2020-10-19, from [https://agupubs](https://agupubs.onlinelibrary.wiley.com/doi/abs/10.1029/2019GL085782)
682 [.onlinelibrary.wiley.com/doi/abs/10.1029/2019GL085782](https://agupubs.onlinelibrary.wiley.com/doi/abs/10.1029/2019GL085782) (eprint:
683 <https://agupubs.onlinelibrary.wiley.com/doi/pdf/10.1029/2019GL085782>) doi:
684 10.1029/2019GL085782
685 Zelinka, M. D., Smith, C. J., Qin, Y., & Taylor, K. E. (2023, August). Comparison
686 of methods to estimate aerosol effective radiative forcings in climate models.
687 *Atmospheric Chemistry and Physics*, 23(15), 8879–8898. Retrieved 2023-08-15,
688 from <https://acp.copernicus.org/articles/23/8879/2023/> (Publisher:
689 Copernicus GmbH) doi: 10.5194/acp-23-8879-2023